Biosensors and Bioelectronics 133 (2019) 94–99

Contents lists available at ScienceDirect

Biosensors and Bioelectronics

journal homepage: www.elsevier.com/locate/bios

Bioinspired synthesis of organic–inorganic hybrid nanoflowers for robust enzyme-free electrochemical immunoassay

Qiaorong Tang[a,1], Lianhua Zhang[c,1], Xiaofeng Tan[a], Lei Jiao[a], Qin Wei[a], He Li[a,b,*]

[a] Institute of Surface Analysis and Chemical Biology, School of Chemistry and Chemical Engineering, University of Jinan, Jinan 250022, China
[b] College of Optoelectronics Technology, Chengdu University of Information Technology, Chengdu 610225, China
[c] Renji Hospital, Shanghai Jiao Tong University School of Medicine, Shanghai 200127, China

ARTICLE INFO

Keywords:
Organic-inorganic hybrid nanoflower
Biomimetic mineralization
Enzyme-free
Electrochemical immunosensor

ABSTRACT

Protein-inorganic nanoflowers have been extensively used for sensing and biosensing applications by virtue of the signal enhancement of protein component—enzyme. Can the inorganic component of protein-inorganic nanoflowers be employed to amplify signal transducing for enzyme-free detection? In this work, a new kind of BSA-antibodies-copper phosphate hybrid nanoflowers (BSA-Ab_2-$Cu_3(PO_4)_2$) has been prepared by one-pot biomimetic mineralization process as signal enhancer for enzyme-free electrochemical immunoassay. C-reactive protein (CRP) has been chosen as a model biomarker. To the best of our knowledge, it is the first trial using the inorganic component—phosphate ions of BSA-Ab_2-$Cu_3(PO_4)_2$ for transducing electrochemical readout, which features the following advantages: (1) the three-dimensional hierarchical porous nanoflower morphology with a high specific surface area could load more antibodies, and BSA for blocking non-specific sites, greatly increasing the sensitivity of the fabricated immunosensors, (2) the $Cu_3(PO_4)_2$ hybrid nanoflowers can supply a huge amount of phosphate anions to react with molybdate yielding molybdophosphate precipitates and generating redox currents for more robust enzyme-free electrochemical signal readout. The fabricated immunosensor has exhibited good detection performance with a linear range of 5 pg/mL–1 ng/mL and a limit of detection of 1.26 pg/mL. Moreover, our method has presented good feasibility for clinical sample analysis.

1. Introduction

It is always gained extensive research interest to develop efficient methods for sensitive and reliable detection of protein biomarkers. Many immunoassay approaches have been explored, such as colorimetric (Shao et al., 2018), fluorescent (Chen et al., 2018), chemiluminescent (Im et al., 2017) and electrochemical methods (Akanda and Ju, 2018). It is well worth to mention that electrochemical immunoassay has become a popular methodology by the inherited advantages of cost efficiency, easy operation, fast response and high sensitivity (Chikkaveeraiah et al., 2012; Felix and Angnes, 2018). Among them, enzyme induced signal amplification strategy has been well adopted (Hou et al., 2018; Mani et al., 2009; Li et al., 2017). Especially, enzyme-linked immunosorbent assay (ELISA) has been taken as the most popular method for sensitive detection of protein biomarkers in clinical lab (Wu and Qu, 2015). The key issue is to develop efficient way to immobilize as many more enzymes as possible and simultaneously keep or even enhance the activity and stability.

Learning from nature always gives great opportunity to pave the way for the advancement of science and technology in many fields (Munch et al., 2008; Lee et al., 2007; Huh et al., 2007). The new developed biomimetic mineralization methodology to prepare protein-inorganic hybrid nanoflowers has become an elegant way for protein immobilization by the facile, mild and green preparation procedure. (Ge et al., 2012). According to this strategy, various enzymes such as laccase (Batule et al., 2015; Cao et al., 2015), horseradish peroxidase (Lin et al., 2014b; Li et al., 2016a), glucose oxidase (Sun et al., 2014; Ariza-Avidad et al., 2016; Li et al., 2016b), protease (Zhang et al., 2015) and papain were immobilized with metal phosphates to produce a diversity of hybrid nanoflowers often achieving improved activity, stability (Zhang et al., 2016a) or durability. And then some trials have been made for immunoassay improved by protein-inorganic hybrid nanoflowers. We prepared a new kind of “all-in-one” concanavalin A-glucose oxidase-$CaHPO_4$ hybrid nanoflowers (Con A-GOx-$CaHPO_4$)

* Corresponding author at: Institute of Surface Analysis and Chemical Biology, School of Chemistry andChemical Engineering, University of Jinan, Jinan 250022, China.
E-mail address: lihecd@gmail.com (H. Li).
[1] These authors contributed equally to this work.

https://doi.org/10.1016/j.bios.2019.03.032
Received 2 September 2018; Received in revised form 10 March 2019; Accepted 17 March 2019
Available online 18 March 2019
0956-5663/

containing the recognition unit of Con A for recognizing *Escherichia coli* O157:H7 and the signal amplification unit of GOx, which has been utilized to detect of food pathogen through relevant change in pH (Ye et al., 2016). A dual-function hybrid nanoflower of streptavidin-HRP-$Cu_3(PO_4)_2$ was also reported by introduced streptavidin for capturing the biotinylated antibody, and HRP for signal enhancement which was employed for colorimetric immunoassay of alpha-fetoprotein (Liu et al., 2017). It should be mentioned that the shortcomings are still not negligible. Enzyme which serves as necessary for the catalytic amplification process means that signal probe is susceptible to specific harsh detection conditions, which will sacrifice the catalytic activity by enzyme denaturation. Consequently, can we make fully use of the advantages of biomimetic mineralization methodology into the fabrication of electrochemical immunosensors?

It will be an advisable choice to develop enzyme-free immunoassay methodology. Some excited achievements have been made for enzyme-free immunoassay of protein biomarkers by pressure, thermal, colorimetric, fluorescent and electrochemical readout (Li et al., 2018a, 2018b, 2018c; Zhang et al., 2018a, 2018b, 2018c; Xia et al., 2015; Miao et al., 2018). Among them, electrochemical methods have gained significant research interest for the inherited merits of fast response, cost effective and high sensitivity (Zhang et al., 2018a, 2018b; Deng et al., 2018). Recently, some detection methods based on tracing phosphate ions (Pi) as signal probes have been proposed. Pi originating from the DNA (or other nucleic acids) phosphate backbone which serve as redox mediators could react with molybdates to induce redox electric current (Xie et al., 2015; Hu et al., 2017; Jiang et al., 2017). Inspired by those fascinated work, we proposed a new kind of BSA-antibodies-copper phosphate hybrid nanoflowers (BSA-Ab_2-$Cu_3(PO_4)_2$) by one-pot biomimetic mineralization methodology for electrochemical immunoassay of C-reactive protein (CRP) based on the following considerations: 1) the mild bioinspired procedure will do great beneficial for maintaining the biocognition activity of antibodies; 2) the inorganic component of $Cu_3(PO_4)_2$ can supply a huge amount of phosphate anions to react with molybdate yielding molybdophosphate precipitates and generating redox currents for more reliable enzyme-free electrochemical signal readout; 3) Due to large specific surface area of nanoflowers, they can load many antibodies, and BSA for blocking non-specific sites, greatly increasing the sensitivity of the fabricated immunosensors.

2. Experimental section

2.1. Reagents and apparatus

Reagents and apparatus used are presented in Supplementary Materials.

2.2. Preparation of polydopamine nanospheres (PDANS)

The preparation of PDANS can be seen in Supplementary Materials.

2.3. One-pot synthesis of BSA-Ab_2-$Cu_3(PO_4)_2$ nanoflowers as signal labels

As shown in Scheme 1**A**, the BSA-Ab_2-$Cu_3(PO_4)_2$ hybrid nanoflowers were prepared by one-pot bio-mineralization process with some modifications. (Ge et al., 2012; Wei et al., 2016). Typically, 100 μL of BSA (1 mg mL^{-1}) and 150 μL of CRP-Ab_2 (100 μg mL^{-1}) were put into 10 mL of PBS (0.01 M, pH 7.4) for incubation of 0.5 h. Thereafter, 360 μL of $CuSO_4$ solution (100 mM) and 50 μL of 10% KCl solution were added to the above proteins mixed solution, and following incubation at 25 °C for 18 h. Subsequently, the solution was centrifuged (9500 rpm, 15 min) at 4 °C, washed three times with deionized water. Following freeze-dried, the all-in-one nanoflowers were obtained and stored at −20 °C. Eventually, the resulting nanoflowers were freshly redispersed in 4 mL of ultrapure water before use.

2.4. Procedure of electrochemical immunoassay

The fabrication procedure of immunosensor is illustrated in Scheme 1**B**. Briefly, the GCE was polished sequentially with 0.3 and 0.05 mm alumina slurry and washed ultrasonically in ethanol for 5 min to obtain a smooth surface. Subsequently, 6 μL of PDANS (1.0 mg mL^{-1}) were dropped on the surface of the GCE. After drying at room temperature, 6 μL of Ab_1 (100 μg mL^{-1}) was added into PDANS modified electrode for 1 h immobilization at 37 °C. Then 3 μL 1% BSA was added onto the electrode for blocking nonspecific adsorption sites. Afterwards, 6 μL of various concentrations of CRP antigens were pipetted into the electrode surface incubating at 37 °C for 1 h. Successively, 6 μL of BSA-Ab_2-$Cu_3(PO_4)_2$ hybrid nanoflowers (100 μg mL^{-1}) were incubated on electrode for 1 h to finish immune reaction at 37 °C. Subsequently, the unbound signal labels were removed by deionized water washing Finally, an exogenous Na_2MoO_4 solution (6 μL, 6 mM) was dropped on the electrode surface for 30 min for electrochemical measurement in 0.5 M H_2SO_4.

3. Results and discussion

3.1. Characterizations of BSA-Ab_2-$Cu_3(PO_4)_2$ hybrid nanoflowers and PDANS

BSA-Ab_2-$Cu_3(PO_4)_2$ hybrid nanoflowers were synthesized by a mild biomineralization process based on protein inducing copper phosphate crystal nucleation (Ge et al., 2012; Wei et al., 2016). As revealed by SEM image (Fig. 1**b**), BSA-Ab_2-$Cu_3(PO_4)_2$ hybrids nanoflowers present flower-like structure, delivering three-dimensional hierarchical structures with average size of 5 ± 0.5 μm, which are very similar to a kind of daisy pompon (Fig. 1**A**). The large specific surface area of our synthetic porous nanoflowers could link more antibodies and contain a large amount of phosphate to enhance the sensitivity of the immunosensor (Zeng and Xia, 2012). The XRD analysis was performed to further characterize the inorganic components of BSA-Ab_2-$Cu_3(PO_4)_2$ nanoflowers (Fig. 1**D**). All diffraction peaks are consistent with the feature peaks of $Cu_3(PO_4)_2{\cdot}3H_2O$ (JCPDS Card No.22-0548) (Ye et al., 2016). As observed from the TEM image in Fig. 1**E**, PDANS have uniform sphere-like structure. Further characterization of PDANS was carried out by FTIR (Fig. 1**F**). PDANS have good biocompatibility and provide an ideal interface for immobilized recognition molecules, such as antibodies and aptamers through Michael addition reactions (Zheng et al., 2015; Lin et al., 2014a; Zhang et al., 2016b; Liu et al., 2016). After polymerization, the feature peaks of dopamine from 1800 cm^{-1} to 500 cm^{-1} have disappeared, which is consistent with previous reports (Jiao et al., 2017).

3.2. Electrochemical characterization of molybdophosphate precipitate

In this work, massive phosphate anions in biomineralized BSA-Ab_2-$Cu_3(PO_4)_2$ organic-inorganic hybrids nanoflowers can react efficiently with molybdates to generate redox-active molybdophosphate precipitate under acid conditions (Hu et al., 2017; Jiang et al., 2017). The reaction on the formation of molybdophosphate has been described in Eq. 1. As presented in Fig. 2**A**, when BSA-Ab_2-$Cu_3(PO_4)_2$ nanoflowers and sodium molybdate (6 mM) were simultaneously deposited on PDANS modified electrode surface, the cyclic voltammograms (CV) exhibited two distinct redox peaks at about 0.34 V and 0.14 V, respectively (green line). The two pairs of redox peaks of molybdophosphate appearing at 0.34 V and 0.14 V were attributed to the electron transfer of Mo in molybdophosphate. The involved redox reactions have been presented in Eqs. 2 and 3, respectively. In comparison, when control experiments were carried on only BSA-Ab_2-$Cu_3(PO_4)_2$ nanoflowers or molybdate modified electrode, no obvious redox current signals were appeared (red curve and blue curve). These observations confirmed that only molybdophosphate ($PMo_{12}O_{40}$) precipitates could produce redox

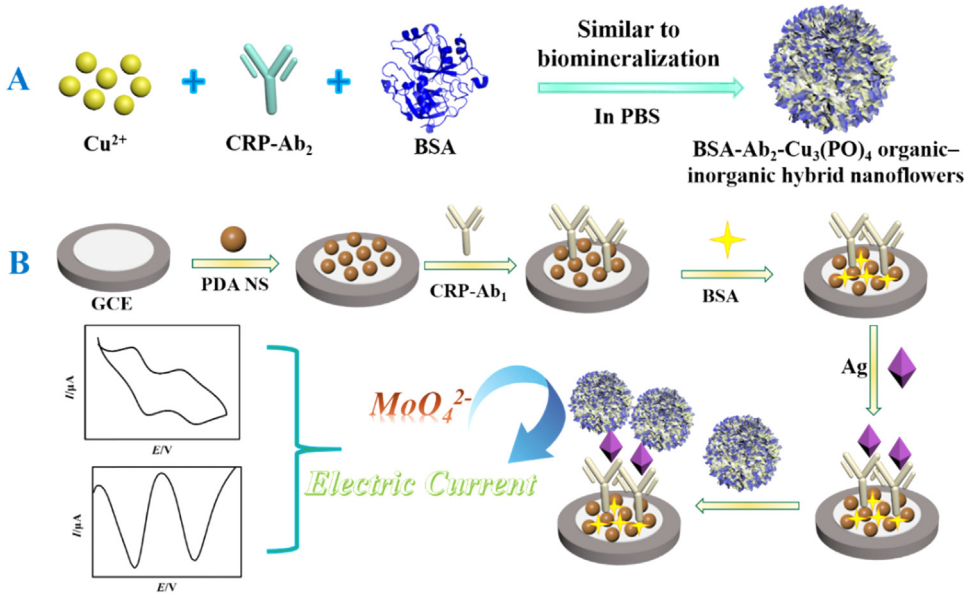

Scheme 1. Illustration the synthesis procedure of BSA-Ab_2-$Cu_3(PO_4)_2$ hybrid nanoflowers as signal labels (A) and the fabrication process of the electrochemical immunosensor (B).

currents due to the different valence states of Mo electron transfer, which fitting well with the previous reports, (Shen et al., 2016; Xie et al., 2015; Li et al., 2018a, 2018b, 2018c).

$$12MoO_4^{2-} + 24H^+ + PO_4^{3-} \rightarrow PMo_{12}O_{40}^{3-} + 12H_2O \quad (1)$$

$$PMo_{12}O_{40}^{3-} + 2e^- + 2H^+ \rightarrow H_2PMo_2{}^{V}Mo_{10}{}^{VI}O_{40}^{3-} \quad (2)$$

$$H_2PMo_2{}^{V}Mo_{10}{}^{VI}O_{40}^{3-} + 2e^- + 2H^+ \rightarrow H_4PMo_2{}^{V}Mo_8{}^{VI}O_{40}^{3-} \quad (3)$$

As shown in Fig. 2**B**, square wave voltammetry (SWV) measurements also confirmed the generating redox active molybdophosphate precipitates. The electrochemical immunosensors were prepared fabricated to detect blank control sample without CRP (curve a) and CRP (curve b). When the system was added to molybdate, the peak current of the curve b was significantly higher than that of curve a. The resulting peak current was ascribed to the reaction with molybdate by BSA-Ab_2-$Cu_3(PO_4)_2$ hybrid nanoflowers, which were captured by the specific binding between the antibody of BSA-Ab_2-$Cu_3(PO_4)_2$ hybrid nanoflowers and CRP immobilized on the electrode.

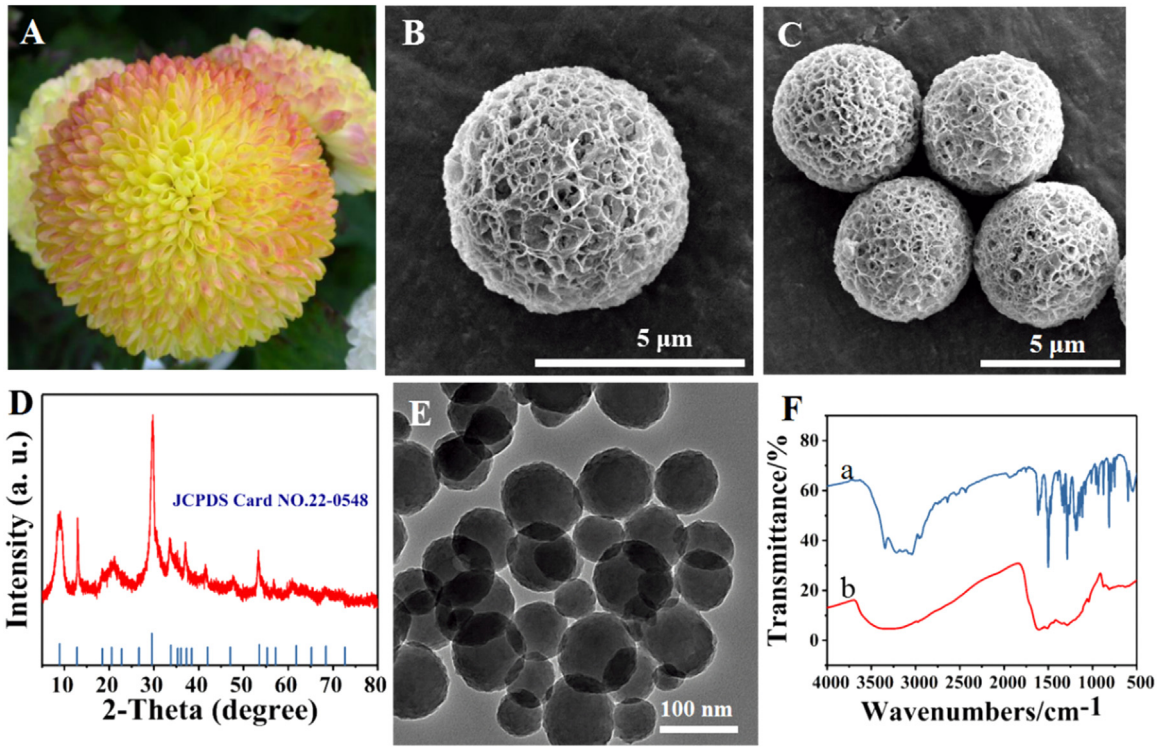

Fig. 1. The photo of pompon flowers (A); the SEM image of BSA-Ab_2-$Cu_3(PO_4)_2$ nanoflowers (B), (C); the XRD pattern of BSA-Ab_2-$Cu_3(PO_4)_2$ nanoflowers (D); the TEM image of PDANS (E); FT-IR spectra of dopamine hydrochloride (a) and PDANS (b) (F).

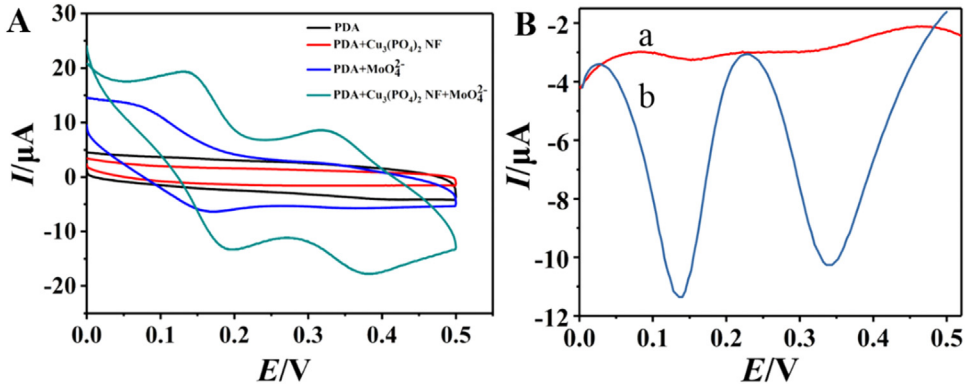

Fig. 2. CV of PDANS modified electrode (black line), BSA-Ab_2-$Cu_3(PO_4)_2$ nanoflowers on the modified electrode (red line), and sodium molybdate reaction with (green line), without BSA-Ab_2-$Cu_3(PO_4)_2$ nanoflowers on the modified electrode (blue line) (A); SWV curves of the detection in absence of CRP (a) and for containing CRP (b) (B); in 0.5 M H_2SO_4. (For interpretation of the references to color in this figure legend, the reader is referred to the web version of this article)

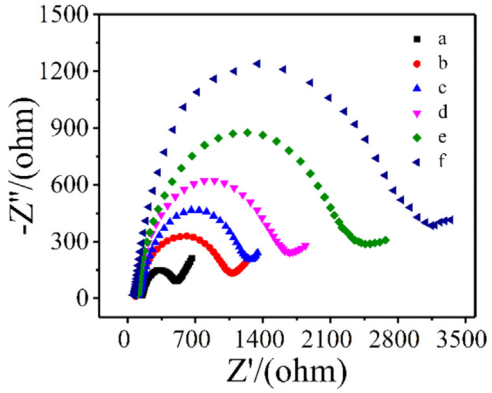

Fig. 3. EIS responses recorded at different modified electrodes in 5.0 mM $[Fe(CN)_6]^{3-/4-}$ and 0.1 M KCl. From curve a to curve f: bare GCE; PDANS/GCE; Ab_1/PDA NS/GCE; BSA/Ab_1/PDANS/GCE; CRP/BSA/Ab_1/PDANS/GCE; BSA-Ab_2-$Cu_3(PO_4)_2$/CRP/BSA/Ab_1/PDANS/GCE, respectively.

3.3. Characterization of the electrochemical immunosensor

Electrochemical impendence spectrum (EIS) as an effective tool was performed to characterize the assembled process of the electrochemical immunosensor (Ma et al., 2016; Dai et al., 2015), which consists of the linear portion low frequencies and the semicircular portion at high frequencies. The diameter of the semicircle is approximately to the impedance of the electrode (Li et al., 2018a, 2018b, 2018c). It can be seen from Fig. 3 that the impedance changes clearly following the modification process of the electrode surface layers. Compared with bare GCE (curve a), electron transfer resistance all increased continuously after the immobilization of Ab_1, BSA, CRP and BSA-Ab_2-$Cu_3(PO_4)_2$ nanoflowers successively (curve c-f). The increase in the impedance indicates that the added proteins as biomacromolecules hinder the transfer of electrons. Therefore, the immunosensor assembly process is successful.

3.4. Analytical performance of the immunosensor

Under the optimal conditions (Fig. S1), different concentrations of CRP range from 5 pg mL^{-1} to 1 ng mL^{-1} were measured by the electrochemical immunosensors. As illustrated in the Fig. 4**A**, the SWV peak currents of the immunosensors increased following the concentration of CRP increased at + 0.14 V and + 0.34 V, respectively. The main reason was that more BSA-Ab_2-$Cu_3(PO_4)_2$ nanoflowers would be captured on the electrode with the increase of CRP. Due to the specific binding between CRP and the antibody of the nanoflowers label, the nanoflowers could react with molybdate yielding molybdophosphate precipitates for generating higher redox currents. As presented in Fig. 4**B,** the peak current signals at +0.14V were adopted for immunoassay because of the better linear coffiecient, when compared with the peak current signals at +0.34V (insert). Accordingly, the calibration curve of CRP was determined as $Y = -4.709–3.902 * X$ ($R^2 = 0.987$) with the limit of detection (LOD) of 1.26 pg mL^{-1}.

As compared with some reported results for detecting CRP, the presented enzyme-free electrochemical immunoassay exhibited more sensitive detection performance (Table S1). The outstanding detection performance of our work can be attributed to the following features: (1) the three-dimensional hierarchical porous nanoflower morphology with a high specific surface area could load more antibodies, and BSA for blocking non-specific sites, greatly increasing the sensitivity of the fabricated immunosensors, (2) the $Cu_3(PO_4)_2$ hybrid nanoflowers can supply a huge amount of phosphate anions to react with molybdate yielding molybdophosphate precipitates and generating redox currents for more robust enzyme-free electrochemical signal readout.

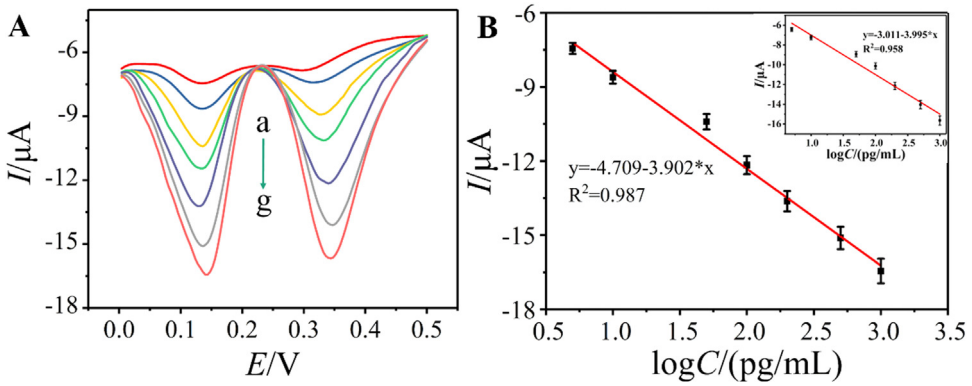

Fig. 4. SWV response (A); calibration curve at 0.14 V (B) and at 0.34 V (insert) of the developed electrochemical immunosensor towards different concentrations of CRP (5, 10, 50, 100, 200, 500, 1000 pg mL^{-1}) in 0.5 M H_2SO_4.

Table 1
Assay results of serum samples based on immunoturbidimetric assay in hospital and the developed electrochemical method.

Method	Detection (μg/mL)	$\bar{d}$ (μg/mL)	S_d	$t_{calculated}$
Immunoturbidimetric assay	0.81, 0.63, 0.21, 1.34, 3.63, 6.00, 18.20, 11.60	− 0.278	0.549	1.432
This developed method	0.83, 0.60, 0.28, 1.44, 3.56, 6.12, 17.13, 10.24			

$\bar{d}$: the mean value of the differences.
S_d: standard deviation of the differences.
The tabulated student's *t* value at 95% confidence is 2.365.

3.5. Application in the analysis of serum samples

The developed electrochemical immunosensors exhibited good enough specificity and reproducibility (Fig. S2). Naturally, we would like to evaluate the feasibility of our method for real sample analysis. We detected the CRP levels in serum samples of eight donors (four healthy people and four patients). CRP levels in serum of healthy individuals usually are less than 3 μg mL^{-1} (Ji et al., 2016). We adopted the fabricated robust enzyme-free electrochemical immunosensors for the measurements and compared the results by immunoturbidimetric method supplied by Ren Ji Hospital, Shanghai Jiao Tong University School of Medicine, using a students's *t*-test. As listed in Table 1, there is no significantly statistical difference between our electrochemical method and the immunoturbidimetric assay by the hospital ($t_{calculated} < t_{table}$) (Harris, 2010a, 2010b.). Thus, our method possesses high accuracy and good reliability, which can be applied in the clinical analysis.

4. Conclusion

In summary, we described a mild one-pot process for the preparation of BSA-Ab_2-$Cu_3(PO_4)_2$ nanoflowers, which were employed to construct the enzyme-free electrochemical immunosensors. The advantages of the fabricated immunosensors can be highlighted to the following aspects: (1) BSA-Ab_2-$Cu_3(PO_4)_2$ organic-inorganic nanoflowers integrate the functions of biorecognition and signal amplification; (2) the signal enhancement is mainly attributed to the abundant phosphate ions in BSA-Ab_2-$Cu_3(PO_4)_2$ nanoflowers can yield a great deal of electrochemical active molybdophosphates by reacting with molybdate; (3) positive working potential (+0.14 V) is chosen for electrochemical immunoassay, which can effectively avoid the interferences from dissolved oxygen during electrochemical measurements. The developed methodology demonstrated good robustness and feasibility for potential clinical usage.

CRediT authorship contribution statement

Qiaorong Tang: Validation, Formal analysis, Writing - original draft. **Lianhua Zhang:** Methodology, Formal analysis, Writing - original draft. **Xiaofeng Tan:** Methodology, Investigation. **Lei Jiao:** Formal analysis. **Qin Wei:** Methodology, Investigation. **He Li:** Conceptualization, Writing - review & editing, Supervision.

Acknowledgements

This work was supported by the National Natural Science Foundation of China (No. 21245007 and 81000976), and the Natural Science Foundation of Shandong Province (No. ZR2017MB017). We also gratefully acknowledge the support from the One-Thousand-Talents Scheme in Sichuan Province.

Declaration of interest statement

We declare that we do not have any commercial or associative interest that represents a conflict of interest in connection with the work submitted.

Appendix A. Supporting information

Supplementary data associated with this article can be found in the online version at doi:10.1016/j.bios.2019.03.032.

References

Akanda, Md.R., Ju, H., 2018. Anal. Chem. 90, 8028–8034.
Ariza-Avidad, M., Salinas-Castillo, A., Capitan-Vallvey, L.F., 2016. Biosens. Bioelectron. 77, 51–55.
Batule, B.S., Park, K.S., Kim, M.I., Park, H.G., 2015. Int. J. Nanomed. 10, 137–142.
Cao, H., Yamg, D., Ye, D., Zhang, X., Fang, X., Zhang, S., Liu, B., Kong, J., 2015. Biosens. Bioelectron. 68, 329–335.
Chen, C., Zhao, J., Lu, Y., Sun, J., Yang, X., 2018. Anal. Chem. 90, 3505–3511.
Chikkaveeraiah, B., Bhirde, A., Morgan, N., Eden, H., Chen, X., 2012. ACS Nano 6, 6546–6561.
Dai, H., Xu, G., Zhang, S., Hong, Z., Lin, Y., 2015. Chem. Commun. 51, 7697–7700.
Deng, C., Zhang, M., Liu, C., Deng, H., Huang, Y., Yang, M., Xiang, Y., Ren, B., 2018. Anal. Chem. 90, 11446–11452.
Felix, F.S., Angnes, L., 2018. Biosens. Bioelectron. 102, 470–478.
Ge, J., Lei, J., Zare, R.N., 2012. Nat. Nanotechnol. 7, 428–432.
Harris, D.C., 2010a. 8th edition. Quantitative Chemical Analysis 98 W. H. Freeman & Company, New York, USA.
Harris, D.C., 2010b. W. H. Freeman and Company: New York, 8th ed..
Hou, Y., Wang, J., Jiang, Y., Lv, C., Xia, L., Hong, S., Lin, M., Lin, Y., Zhang, Z., Pang, D., 2018. Biosens. Bioelectron. 99, 186–192.
Huh, D., Mills, K.L., Zhu, X.Y., Burns, M.A., Thouless, M.D., Takayama, S., 2007. Nat. Mater. 6, 424–428.
Hu, L., Hu, S., Guo, L., Shen, C., Yang, M., Rasooly, A., 2017. Anal. Chem. 89, 2547–2552.
Im, J., Kim, H., An, B., Chang, Y., Kang, M., Lee, T., Son, J., Park, J., Pyun, J., 2017. Biosens. Bioelectron. 92, 221–228.
Ji, T.H., Liu, D., Liu, F., Li, J.X., Ruan, Q.Y., Song, Y.L., Tian, T., Zhu, Z., Zhou, L.Z., Lin, H., Yang, C.Y., Wang, D., 2016. Chem. Commun. 52, 8452–8454.
Jiang, W., Tian, D., Zhang, L., Guo, Q., Cui, Y., Yang, M., 2017. Microchim Acta 184, 1–7.
Jiao, L., Xu, Z., Du, W., Li, H., Yin, M., 2017. ACS Appl. Mater. Interfaces 9, 28339–28345.
Lee, H., Lee, B.P., Messersmith, P.B., 2007. Nature 448, 338–341.
Li, D., Cui, Y., Morisseau, C., Gee, S.J., Bever, C.S., Liu, X., Wu, J., Hammock, B.D., Ying, Y., 2017. Anal. Chem. 89, 6248–6256.
Li, M., Luo, M., Li, F., Wang, W., Liu, K., Liu, Q., Wang, Y., Lu, Z., Wang, D., 2016a. J. Phys. Chem. C. 120, 17348–17356.
Li, F., Li, Y., Feng, J., Gao, Z., Lv, H., Ren, X., Wei, Q., 2018a. Biosens. Bioelectron. 100, 512–518.
Li, J., Liu, F., Zhu, Z., Liu, D., Chen, X., Song, Y., Zhou, L., Yang, C., 2018b. ACS Appl. Mater. Interfaces 10, 13390–13396.
Li, X., Shen, C., Yang, M., Rasooly, A., 2018c. Anal. Chem. 90, 4764–4769.
Li, Z., Ding, Y., Li, S., Jiang, Y., Liu, Z., Ge, J., 2016b. Nanoscale 8, 17440–17445.
Lin, L., Cong, Z., Cao, J., Ke, K., Peng, Q., Gao, J., Yang, H., Liu, G., Chen, X., 2014a. ACS Nano 8, 3876–3883.
Lin, Z., Xiao, Y., Yin, Y., Hu, W., Liu, W., Yang, H., 2014b. ACS Appl. Mater. Interfaces 6, 10775–10782.
Liu, D., Ma, L., Liu, L., Wang, L., Liu, Y., Jia, Q., Guo, Q., Zhang, G., Zhou, J., 2016. ACS Appl. Mater. Interfaces 8, 24455–24462.
Liu, Y., Chen, J., Du, M., Wang, X., Ji, X., He, Z., 2017. Biosens. Bioelectron. 92, 68–73.
Ma, H., Li, Y., Wang, Y., Hu, L., Zhang, Y., Fan, D., Yan, T., Wei, Q., 2016. Biosens. Bioelectron. 78, 167–173.
Mani, V., Chikkaveeraiah, B., Patel, V., Gutkind, J.S., Rusling, J.F., 2009. ACS Nano 3, 585–594.
Miao, L., Zhu, C., Jiao, L., Li, H., Du, D., Lin, Y., Wei, Q., 2018. Anal. Chem. 90, 1976–1982.
Munch, E., Launey, M.E., Alsem, D.H., Saiz, E., Tomsia, A.P., Ritchie, R.O., 2008. Science 322, 1516–1520.
Shao, F., Zhang, L., Jiao, L., Wang, X., Miao, L., Li, H., Zhou, F., 2018. Anal. Chem. 90, 8673–8679.
Shen, C., Li, X., Rasooly, A., Guo, L., Zhang, K., Yang, M., 2016. Biosens. Bioelectron. 85, 220–225.
Sun, J., Ge, J., Liu, W., Lan, M., Zhang, H., Wang, P., Wang, Y., Niu, Z., 2014. Nanoscale 6,

255–262.
Wei, T., Du, D., Zhu, M., Lin, Y., Dai, Z., 2016. ACS Appl. Mater. Interfaces 8, 6329–6335.
Wu, L., Qu, X., 2015. Chem. Soc. Rev. 44, 2963–2997.
Xia, X., Zhang, J., Lu, N., Kim, J.M., Ghale, K., Xu, Y., McKenzie, E., Liu, J., Ye, H., 2015. ACS Nano 9, 9994–10004.
Xie, S., Yuan, Y., Chai, Y., Yuan, R., 2015. Anal. Chem. 87, 10268–10274.
Ye, R., Zhu, C., Song, Y., Lu, Q., Ge, X., Yang, X., Zhu, M., Du, D., Li, H., Lin, Y., 2016. Small 12, 3094–3100.
Zeng, J., Xia, Y.N., 2012. Nat. Nanotechnol. 7, 415–416.
Zhang, B., Li, P., Zhang, H., Fan, L., Wang, H., Li, X., Tian, L., Ali, N., Ali, Z., Zhang, Q., 2016a. RSC Adv. 6, 46702–46710.
Zhang, D., Li, W., Ma, Z., 2018a. Biosens. Bioelectron. 109, 171–176.
Zhang, G., Shan, D., Dong, H., Cosnier, S., Al-Ghanim, K.A., Ahmad, Z., Mahboob, S., Zhang, X., 2018b. Anal. Chem. 90, 12284–12291.
Zhang, J., Xing, H., Lu, Y., 2018c. Chem. Sci. 9, 3906–3910.
Zhang, L., Su, H., Cai, J., Cheng, D., Ma, Y., Zhang, J., Zhou, C., Liu, S., Shi, H., Zhang, Y., Zhang, C., 2016b. ACS Nano 10, 10404–10417.
Zhang, Z., Zhang, Y., Song, R., Wang, M., Yan, F., He, L., Feng, X., Fang, S., Zhao, J., Zhang, H., 2015. Sens. Actuator B Chem. 211, 310–317.
Zheng, R., Wang, S., Tian, Y., Jiang, X., Fu, D., Shen, S., Yang, W., 2015. ACS Appl. Mater. Interfaces 7, 15876–15884.